Optimizing Interface Conductivity in Electronics

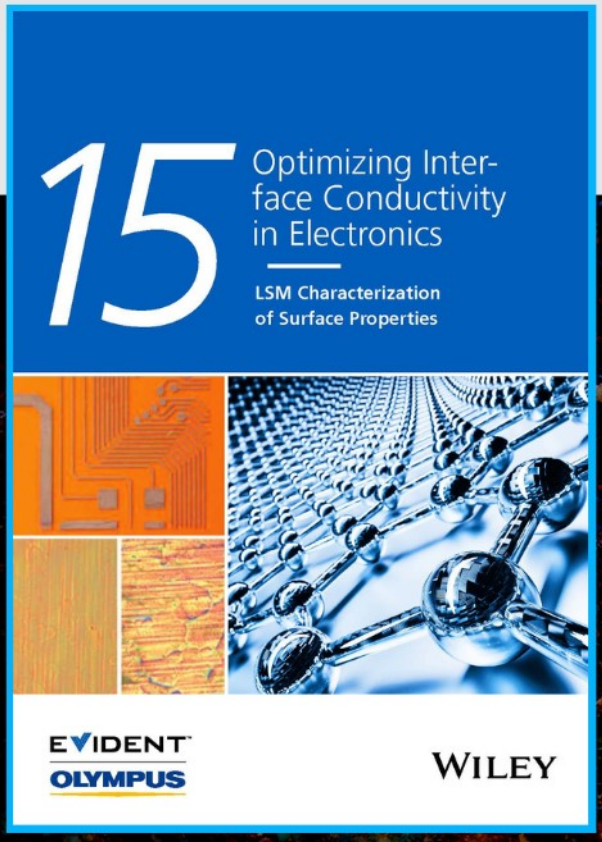

The latest eBook from Advanced Optical Metrology. Download for free.

Surface roughness is a key parameter for judging the performance of a given material's surface quality for its electronic application. A powerful tool to measure surface roughness is 3D laser scanning confocal microscopy (LSM), which will allow you to assess roughness and compare production and finishing methods, and improve these methods based on mathematical models.

Focus on creating high-conductivity electronic devices with minimal power loss using laser scanning microscopy is an effective tool to discern a variety of roughness parameters.

EVIDENT
OLYMPUS

WILEY

ADVANCED FUNCTIONAL MATERIALS
www.afm-journal.de

Catalyst-Free Synthesis of Few-Layer Graphdiyne Using a Microwave-Induced Temperature Gradient at a Solid/Liquid Interface

Chen Yin, Jiaqiang Li, Tianran Li, Yue Yu, Ya Kong, Peng Gao, Hailin Peng, Lianming Tong, and Jin Zhang**

Graphdiyne (GDY), a 2D carbon allotrope, is predicted to possess high carrier mobility and an intrinsic bandgap. However, the controlled synthesis of mono- or few-layer GDY with good crystallinity remains challenging because of the instability of the monomers. Herein, a rapid and catalyst-free synthetic method is presented for few-layer GDY involving the use of a solid/liquid interface and a microwave-induced temperature gradient. Sodium chloride, which can absorb microwave energy, is used as the solid substrate in a nonabsorbing solvent. A temperature gradient is formed at the solid/liquid interface under microwave irradiation, facilitating the cross-coupling reaction of monomers at the solid surface and stabilizing the monomers in the bulk solution. Few-layer GDY with an average thickness of less than 2 nm, a field-effect mobility of 50.1 $cm^2 V^{-1} s^{-1}$, and p-type characteristics is successfully obtained. This wet chemical approach may be extended to the synthesis of other few-layered 2D materials with improved quality.

1. Introduction

Graphdiyne (GDY) is unique among nanocarbon allotropes such as fullerene,[1] carbon nanotubes,[2] and graphene[3] owing to the presence of sp- and sp^2-hybridized carbon atoms in its 2D structure.[4] Since its discovery, GDY has drawn tremendous research attention due to its unique physical and structural properties, such as high carrier mobility, intrinsic electronic bandgap, and uniform topological pores,[5–13] and has shown great potential for various applications such as water/oil separation,[14] catalysis,[15–19] and energy storage.[20]

Several methods for the synthesis of GDY have been reported. The first experimental synthesis of GDY film in 2010 was achieved using an in situ Glaser coupling reaction on a copper substrate.[21] A modified Glaser coupling reaction was adopted by Zhou et al. to synthesize GDY nanowalls.[22] In 2017, Zuo et al. used an explosion method to obtain GDY powders within several seconds.[23] However, although the temperatures of these synthetic processes are high enough for the coupling reaction, the monomer molecules are unstable at such temperatures, leading to side reactions and defects in the GDY. In 2018, Gao et al. developed a solution-phase van der Waals epitaxial method to synthesize ultrathin GDY films on graphene.[24] The epitaxial growth was carried out at room temperature so that the hexaethynylbenzene (HEB) monomers remained stable and GDY with improved crystallinity was obtained. However, it proved difficult to separate the GDY film from the graphene. Typically, wet chemical synthesis of 2D materials requires involved and time-consuming postprocess to removing either catalyst residue components or by-products prior to characterization and/or further applications, and such processes can cause product defects and degradation.[25,26]

Herein, we report a rapid and catalyst-free synthetic method for ultrathin GDY film that exploits a microwave-induced temperature gradient at a solid/liquid interface. We chose NaCl as the solid substrate as it can absorb microwave energy, and the HEB is dissolved in a mixture of toluene and hexane, which is a non-microwave-absorbing solvent system. Under microwave irradiation, the NaCl is heated to a certain temperature while the solvent remains unheated so that a temperature gradient is formed at the solid/liquid interface. Thus, the coupling reaction occurs only at the surface of the NaCl, and the HEB monomers in the bulk solution remain stable and can diffuse to the solid/liquid interface intact. As a result, GDY films with an average thickness of less than 2 nm can be obtained. Spectral characterization by Raman scattering spectroscopy, X-ray photoelectron spectroscopy (XPS), and transmission electron

C. Yin
Academy for Advanced Interdisciplinary Studies
Peking University
Beijing 100871, P. R. China

C. Yin, Dr. J. Li, T. Li, Y. Yu, Y. Kong, Prof. H. Peng, Prof. L. Tong, Prof. J. Zhang
Center for Nanochemistry
Beijing Science and Engineering Center for Nanocarbons
Beijing National Laboratory for Molecular Sciences
College of Chemistry and Molecular Engineering
Peking University
Beijing 100871, P. R. China
E-mail: tonglm@pku.edu.cn; jinzhang@pku.edu.cn

Prof. P. Gao
Electron Microscopy Laboratory
School of Physics, and International Center for Quantum Materials
Peking University
Beijing 100871, P. R. China

The ORCID identification number(s) for the author(s) of this article can be found under https://doi.org/10.1002/adfm.202001396.

DOI: 10.1002/adfm.202001396

 © 2020 WILEY-VCH Verlag GmbH & Co. KGaA, Weinheim

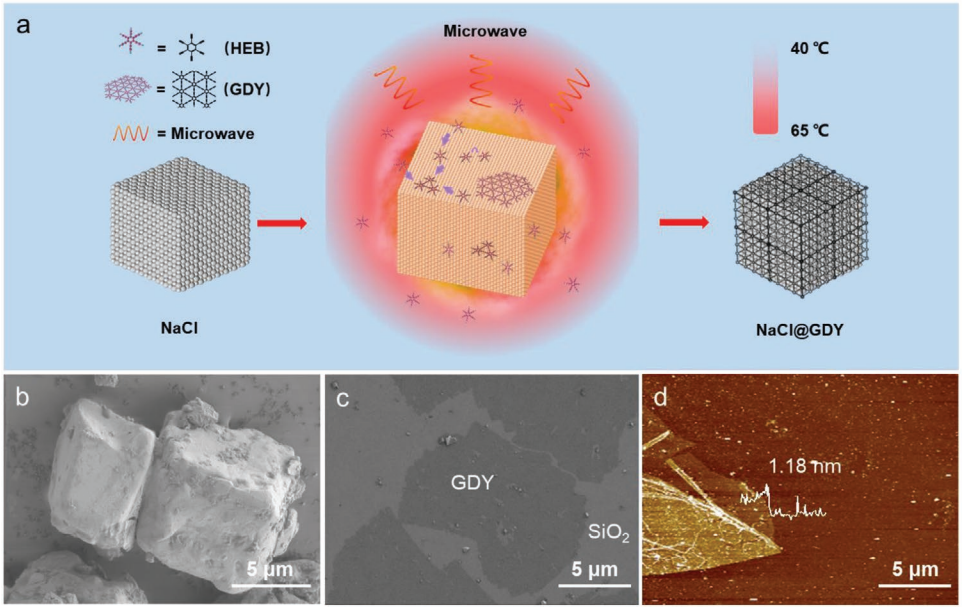

Figure 1. a) Schematic presentation of the synthesis of GDY films. b) SEM image of NaCl@GDY. c) SEM image of GDY films on a SiO_2/Si substrate. d) Typical AFM image of a GDY film.

microscopy (TEM) was used to confirm the structure of the GDY. Furthermore, a field-effect transistor (FET) device based on the GDY film showed a mobility of 50.1 cm^2 V^{-1} s^{-1} and exhibited p-type characteristics.

A schematic of the synthetic processes is given in **Figure 1**a. Briefly, the HEB molecules were dissolved in toluene/hexane (1:1, v/v) at a concentration of 5 mmol. Then, 100 mg of NaCl crystals were added to 30 mL of the HEB solution in a 50 mL polypropylene (PP) centrifuge tube. The reaction system was transferred to a commercial microwave oven and subjected to microwave irradiation at 700 W for 4 min. The temperature of the NaCl increased to ≈70 °C, which is appropriate for the coupling of HEB, as measured by an infrared thermometer.

Microwave-assisted C—H bond activation has been widely used in organic chemistry.[27] In HEB, the C—H dipoles reorient to be in phase with the oscillating electric field. Microwave irradiation to a temperature of 70 °C can promote homolytic cleavage of the terminal alkyne bonds to radicals, which couple to form GDY. However, the temperature of the solvent remains at around 40 °C due to its lower absorption of microwave energy. Therefore, a temperature gradient is formed at the NaCl/solvent interface, spatially confining the alkyne coupling reaction to the surface of the NaCl crystals under a constant supply of stable monomer molecules diffusing from the bulk solution. As a result, thin films of GDY are formed on the surfaces of the cubic NaCl crystals. The GDY and NaCl are then filtered from the solution and washed in acetone several times, whereupon the color of the NaCl changes from white to black (Figure S1, Supporting Information).

A scanning electron microscopy (SEM) image of GDY-covered NaCl crystals (NaCl@GDY) is shown in Figure 1b. Upon mixing the GDY and NaCl with water (2 mg NaCl@GDY in 5 mL H_2O), a GDY dispersion was obtained. A droplet of the GDY dispersion was dropped onto a clean SiO_2/Si substrate, which was then dried in air (Figure S2, Supporting Information). GDY films (see Figure S2, Supporting Information) with widths of 10–20 μm can be clearly observed in the SEM image in Figure 1c. The typical thickness of the film was found to be 1.18 nm by atomic force microscopy (AFM), as shown in Figure 1d, and the thickness analysis is shown in Figure S3 (Supporting Information).

The GDY films were transferred onto a copper grid for TEM characterization. The low-magnification TEM image shows freestanding cubic GDY films with an average width of 200 nm (**Figure 2**a) and typical GDY sheets (Figure 2b). The higher-magnification TEM characterization reveals streaks with widths of 0.368 nm (Figure 2c) at the edges of the thin films, which can be assigned to the spacing between two carbon layers.[28] The high-resolution TEM (HRTEM) images of GDY reveal lattice fringes of 0.468 nm, as shown in Figure 2d, which is in good agreement with theoretical values.[10] Figure 2e shows a magnification of the marked area in Figure 2d, which shows good agreement with the simulated TEM image prepared using quantitative TEM/STEM simulations at the right side.

The structure of the GDY films can be more clearly identified from the corresponding selected area electron diffraction (SAED) patterns in Figure 2f. The (110) diffraction spot for GDY is around 2.1 nm^{-1}, which corresponds to d = 0.47 nm between (110) lattice facets and its equivalent planes. This result matches well with that for GDY with ABC stacking.[29] The energy-dispersive spectroscopy (EDS) results given in Figure S4 (Supporting Information) and the mapping image given in Figure S5 (Supporting Information) show that carbon is the major constituent element. The existence of oxygen could result from adsorption of oxygen from air or inevitable defects, and the copper signal may be due to the copper grid. We also observed twisted GDY films with a twist angle of 17.87° due to the collapse of freestanding cubic GDY films and their subsequent randomly oriented stacking (Figure S6, Supporting Information).

© 2020 WILEY-VCH Verlag GmbH & Co. KGaA, Weinheim

16163028, 2020, 23, Downloaded from https://onlinelibrary.wiley.com/doi/10.1002/adfm.202001396 by Zhejiang University, Wiley Online Library on [04/09/2023]. See the Terms and Conditions (https://onlinelibrary.wiley.com/terms-and-conditions) on Wiley Online Library for rules of use; OA articles are governed by the applicable Creative Commons License

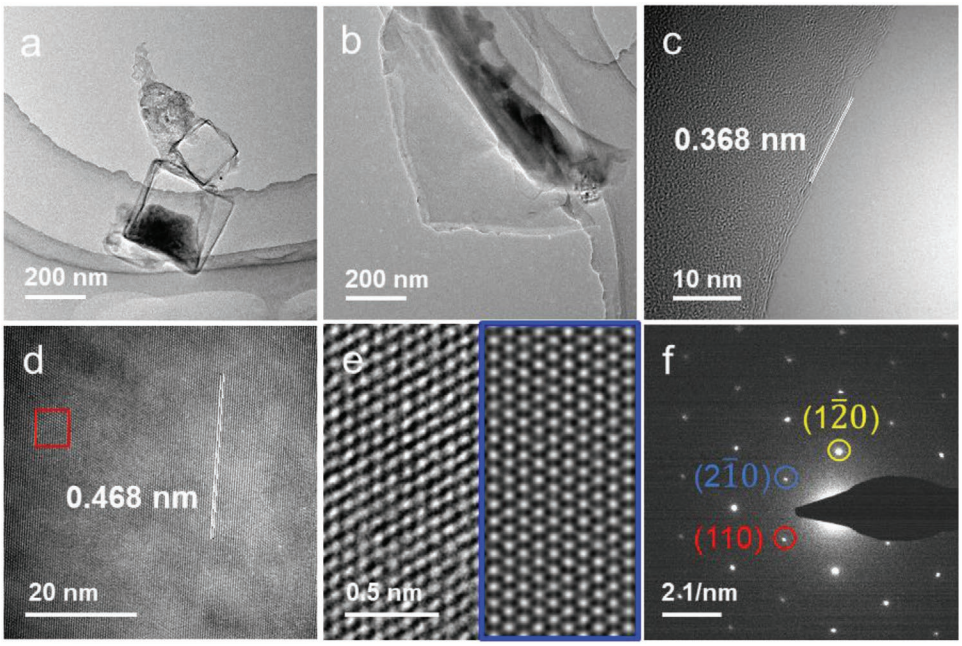

Figure 2. TEM characterization of GDY films. a,b) TEM images of cuboidal GDY boxes and GDY sheets. c,d) HRTEM images of a GDY film. e) Magnification of the area highlighted by the red square in (d). The right hand side of the figure (blue box) shows the corresponding simulated image of GDY with ABC stacking. f) Selected area electron diffraction pattern of GDY film.

The GDY films were further investigated by Raman spectroscopy, XPS, Fourier-transform infrared spectroscopy (FTIR), electron energy loss spectroscopy (EELS), and UV–vis absorption spectroscopy. As shown in **Figure 3**a, the peak at 2177 cm^{-1} that is attributed to the vibration of conjugated diyne chains evidences the successful coupling of alkyne bonds.[21] The peaks at 1415 and 1574 cm^{-1} are assigned to the breathing mode of sp^2-hybridized carbon atoms in aromatic rings (D band) and

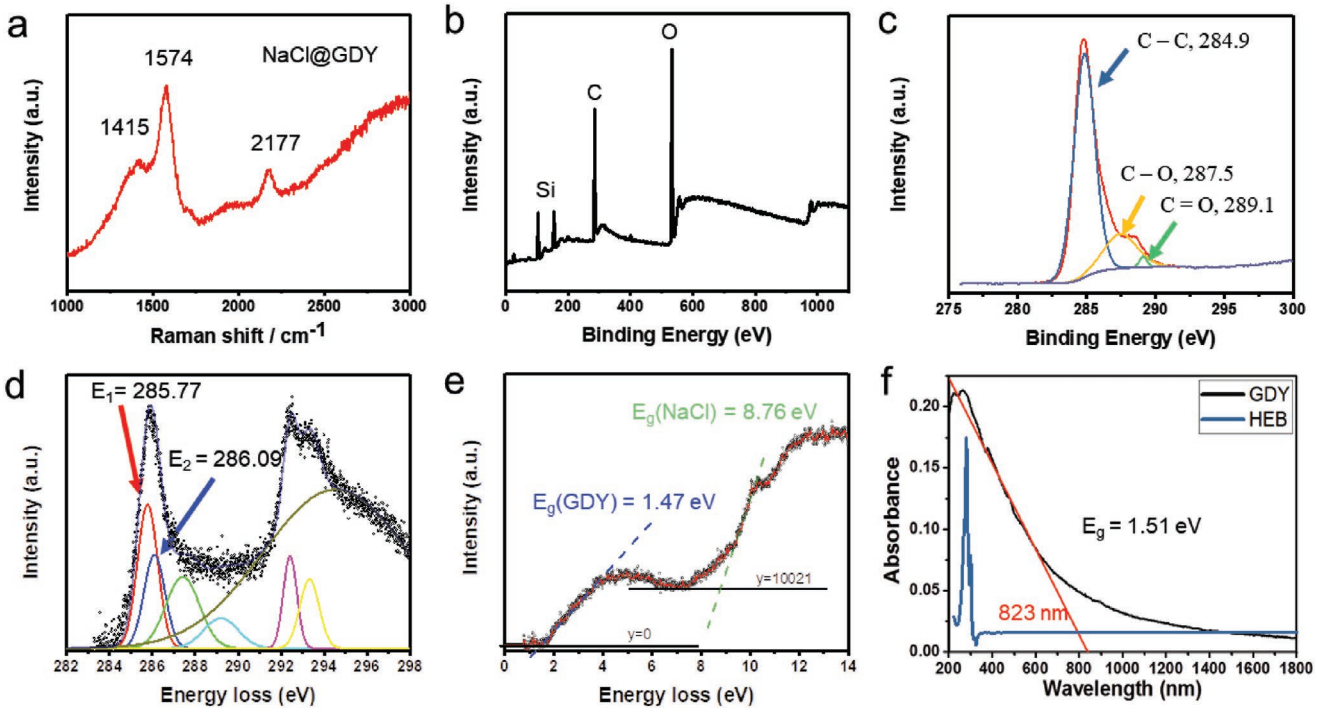

Figure 3. a) Raman scattering, b,c) XPS, and d) ELNES spectra of the GDY films. e) EELS spectrum of GDY films showing a bandgap of ≈1.47 eV for GDY. f) UV–vis absorption spectrum of GDY films and the HEB monomer, in which the red line is a Tauc fitting plot corresponding to an optical bandgap of 1.51 eV.

© 2020 WILEY-VCH Verlag GmbH & Co. KGaA, Weinheim

16163028, 2020, 23, Downloaded from https://onlinelibrary.wiley.com/doi/10.1002/adfm.202001396 by Zhejiang University, Wiley Online Library on [04/09/2023]. See the Terms and Conditions (https://onlinelibrary.wiley.com/terms-and-conditions) on Wiley Online Library for rules of use; OA articles are governed by the applicable Creative Commons License

the first-order mode E_{2g} of in-phase stretching in aromatic rings (G band), respectively.[30] The FTIR spectrum of the synthesized GDY films is shown in Figure S7 (Supporting Information), where four major bands are observed at 1095, 1624, 1698, and 2107 cm^{-1}.

The XPS spectra in Figure 3b,c indicate that the GDY films are mainly composed of carbon. In Figure 3c, the peak for C 1s can be deconvoluted into three subpeaks, corresponding to sp^2- and sp-hybridized carbon atoms, i.e., those in aromatic rings and C≡C bonds, respectively, at binding energies of 284.9 eV, with C—O at 287.5 eV, and C=O at 289.1 eV.[31] In GDY, the number of sp carbons is twice that of sp^2 carbons. Supposing that the detected crystal region has a total of 6n sp^2 carbons and 12n sp carbons, the number of electrons in conjugated π bonds perpendicular to the carbon atom plane is $(3n\Pi_4^4 + n\Pi_6^6)$ and the number of electrons in conjugated π bonds in the carbon atom plane is $3n\Pi_4^4$ (Figure S8, Supporting Information). Thus, the ratio of these two kinds of electrons is 3:2.

The energy-loss near-edge structure (ELNES) results obtained for GDY with an energy resolution of 83.3 meV in Figure 3d indicate that the π^* peak consists of two peaks: the red peak is located at 285.77 eV (C=C) and the blue peak is located at 286.09 eV (C≡C).[32] The area ratio of these two peaks is 3:2, which matches well with the theoretical ratio for GDY discussed above. The other peaks are assigned to C—O (green) at 287.40 eV, C=O (light blue) at 289.14 eV, σ^* (purple) at 292.39 eV, and scattering caused by nearest neighbor atoms (yellow) at 293.33 eV.

The bandgap for the GDY film can be obtained from the EELS spectrum in Figure 3e. It can be seen that the crosspoint abscissa value of the blue dashed line and $y = 0$ is 1.47 eV, which corresponds to the electronic bandgap of GDY and is in good agreement to theoretical model. The crosspoint abscissa value of the green dashed line and $y = 10\,021$ is 8.76 eV, which can be assigned to the bandgap of residual NaCl.[33]

The UV–vis absorption spectra of GDY and HEB were measured in tetrahydrofuran (THF) and are shown in Figure 3f. The background was eliminated by subtracting the signal for an aqueous solution of NaCl and THF. According to Tauc's formulation, the optical bandgap of GDY films was estimated to be 1.51 eV.

The above results confirm that thin films of GDY were successfully obtained through our microwave-assisted coupling reaction. Microwave-assisted/accelerated organic syntheses were first reported in the mid-1980s.[34] Reaction rates and yields can be dramatically enhanced using microwave radiation as a heat source.[35] However, no catalyst was used in our approach, and the activation of the terminal C—H bonds in the HEB monomers and the coupling of alkyne bonds between HEB molecules at the NaCl surfaces are both likely to be facilitated by microwaves.

In order to investigate the mechanism of the coupling reaction, we compared different reaction systems, including 1) HEB solution without NaCl irradiated with microwaves, 2) HEB solution with NaCl homogeneously heated to 70 °C, and 3) HEB solution without NaCl homogeneously heated to 55 °C and then irradiated by microwaves to 70 °C. The results are shown in Figures S9–S11 (Supporting Information). No GDY product is formed in system 1, where the temperature was ≈40 °C after microwave irradiation (Figure S9, Supporting Information), or in system 2, where no NaCl was added (Figure S10, Supporting Information). However, some 0.468 nm lattice fringes are observed for system 3 (Figure S11, Supporting Information), indicating the existence of a very small amount of GDY, although no distinct peak for coupled alkyne bonds is observed in the Raman spectrum.

These results indicate that microwave irradiation and a temperature of 70 °C are both necessary for the efficient coupling of alkyne bonds, and that the temperature gradient at the NaCl/solvent interface ensures the confinement of the coupling reaction and the formation of GDY thin films. As no catalyst was used, the terminal C—H bonds of HEB monomers are expected to be homolytically cleaved to radicals before the coupling reaction.

Furthermore, 2,2,6,6-tetramethylpiperidinyloxy (TEMPO) was added as a radical trap to the reaction system comprising HEB monomers with NaCl in toluene/hexane,[36] and no GDY product was found after microwave irradiation, as shown in Figure S12 (Supporting Information).

For the efficient synthesis of GDY films using microwaves, the dielectric constants of the inorganic crystals and the solvents are determinative factors. Different inorganic salt crystals in toluene/hexane and various organic solvents with different dielectric constants were used for a more detailed comparison (Tables S1 and S2, Supporting Information). The temperatures of the salt crystals and the HEB solvents after microwave irradiation are also listed in Tables S1 and S2 (Supporting Information). An approximately monotonic increase of temperature with dielectric constant is revealed in Figure S13 (Supporting Information).

Although hexane has the lowest dielectric constant of the solvents investigated in our experiments, the solubility of HEB in hexane is too low and the same volume of toluene is necessary to dissolve the HEB monomers. Figure S14 (Supporting Information) shows the Raman spectra of products obtained using different salts in toluene/hexane and those obtained with NaCl in different solvents. It is clear from the results that NaCl crystals (high dielectric constant) in a toluene/hexane solution of HEB (low dielectric constant) are the optimal conditions for the synthesis of thin GDY films at the solid/liquid interface.

Furthermore, the size and thickness of the GDY films can be controlled by altering the duration of microwave irradiation. As shown in Table S3 (Supporting Information), the temperature of the solvent and NaCl increase as the duration of irradiation increases. It can be seen from the SEM images (Figure S15, Supporting Information) of the synthesized GDY films that the size can reach tens of micrometers, and the AFM images in Figure S16 (Supporting Information) show that the thickness can reach ≈4 nm upon 20 min irradiation. The Raman spectra in Figure S17 (Supporting Information) present the peak for a conjugated diyne at 2178 cm^{-1} after 5 min.

The electronic properties of the synthesized few-layer GDY films were investigated using fundamental transport measurements. A schematic of the two-electrode FET device used is shown in **Figure 4**a. An optical image of an FET device with a 2 μm channel width is shown in the inset of Figure 4b. The typical *I–V* characteristic of the few-layer GDY film of 1.5 nm thickness at a bias voltage from −1.00 to +1.00 V in Figure 4b

© 2020 WILEY-VCH Verlag GmbH & Co. KGaA, Weinheim

16163028, 2020, 23, Downloaded from https://onlinelibrary.wiley.com/doi/10.1002/adfm.202001396 by Zhejiang University, Wiley Online Library on [04/09/2023]. See the Terms and Conditions (https://onlinelibrary.wiley.com/terms-and-conditions) on Wiley Online Library for rules of use; OA articles are governed by the applicable Creative Commons License

16163028, 2020, 23, Downloaded from https://onlinelibrary.wiley.com/doi/10.1002/adfm.202001396 by Zhejiang University, Wiley Online Library on [04/09/2023]. See the Terms and Conditions (https://onlinelibrary.wiley.com/terms-and-conditions) on Wiley Online Library for rules of use; OA articles are governed by the applicable Creative Commons License

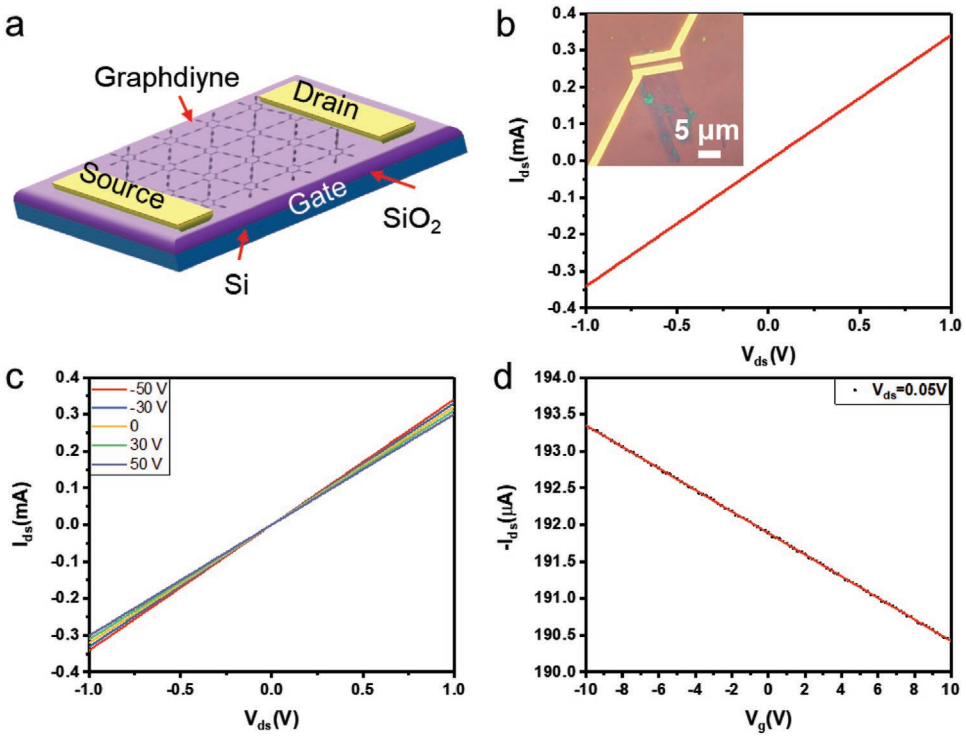

Figure 4. Electrical properties of GDY films. a) 3D schematic view of a GDY transistor. b) I_{ds} versus V_{ds} plot of the device. Inset: optical microscope image of the device. c) I_{ds} versus V_{ds} curves recorded under various V_g biases from −50 to 50 V. d) Transport characteristics curve of the device at V_{ds} = 0.05 V, in which the red line is the linear fitting.

presents a linear relationship, indicating ohmic-like contact between the sample and electrodes and the good conductivity of the GDY film. Figure 4c,d shows the output and transfer characteristics of the device. The p-type semiconducting characteristics of GDY can be inferred from the I_{ds}–V_g curve in Figure 4d. The field-effect mobility of GDY films was calculated to be 50.1 $cm^2\ V^{-1}\ s^{-1}$ using the equation $\mu = [dI/dV_g][L/(WC_gV_{ds})]$,[37] where the channel length (L) is 5 μm, the channel width (W) is 2 μm, and the capacity of gate electrode (C_g) is 1.15 F cm^{-2}.

2. Conclusion

In summary, we have developed a catalyst-free approach to the synthesis of ultrathin GDY films using a microwave-induced temperature gradient at a solid/liquid interface. The monomer molecules only react with each other at the high-temperature interface while nonreacting monomer molecules remain stable in the lower-temperature solvent. The as-synthesized GDY films exhibit smooth and continuous morphology and good crystallinity. The thickness of the as-synthesized GDY films is ≈1–2 nm. HRTEM and SAED analyses revealed the in-plane periodicity of the multilayer GDY, with the SAED pattern exclusively matching an ABC stacking mode. XPS, EDS, Raman, and FTIR spectra presented characteristics consistent with the expected chemical composition and bonding of GDY. Electrical measurements revealed that the GDY films exhibit p-type semiconducting characteristics and a field-effect mobility of 50.1 $cm^2\ V^{-1}\ s^{-1}$. Overall, this work provides a novel and facile strategy for the rapid synthesis of GDY thin films and will benefit the investigation of their fundamental properties and potential application.

3. Experimental Section

Catalyst-Free Synthesis of Few-Layer Graphdiyne Using a Temperature Gradient Solid/liquid Interface: Cubic NaCl crystals with an average size of 10 μm were first obtained by recrystallization of commercial NaCl (average size 300 μm). The HEB was dissolved in toluene/hexane (1:1, v/v) at a concentration of 5 mmol. Then, 100 mg of NaCl crystals were added to 30 mL of the HEB solution in a 50 mL PP centrifuge tube. The reaction system was transferred to a commercial microwave oven and subjected to microwave irradiation at 700 W for 4 min, whereupon thin films of GDY were formed on the surfaces of the cubic NaCl crystals.

Characterization: The morphology and detailed structure of the GDY films were investigated by SEM (Hitachi S-4800, Japan; acceleration voltage 1.0 kV), TEM (FEI Tecnai F30; acceleration voltage 300 kV), and aberration-corrected TEM (NionU-HERMES200 STEM microscope at the Electron Microscopy Laboratory of Peking University; acceleration voltage 60 kV.). Raman spectroscopy (Horiba Jobin Yvon LabRAM HR 800, 514.5 nm), UV–vis spectroscopy (Perkin Elmer Lambda 950), and XPS (Kratos Analytical Axis-Ultra spectrometer with an Al Kα X-ray source) were performed to confirm sample quality.

Supporting Information

Supporting Information is available from the Wiley Online Library or from the author.

© 2020 WILEY-VCH Verlag GmbH & Co. KGaA, Weinheim

Acknowledgements

This work was supported by the Ministry of Science and Technology of the People's Republic of China (2018YFA0703502 and 2016YFA0200104) and the National Natural Science Foundation of China (Grant Nos. 51432002, 51720105003, 21790052, 21573004, 21974004, 51672007, and 11974023).

Conflict of Interest

The authors declare no conflict of interest.

Keywords

catalyst-free, few-layered, graphdiyne, microwave, temperature gradient

Received: February 13, 2020
Revised: February 28, 2020
Published online: April 9, 2020

[1] H. W. Kroto, J. R. Heath, S. C. O'Brien, R. F. Curl, R. E. Smalley, *Nature* **1985**, *318*, 162.
[2] S. Iijima, *Nature* **1991**, *354*, 56.
[3] K. S. Novoselov, A. K. Geim, S. V. Morozov, D. Jiang, Y. Zhang, S. V. Dubonos, I. V. Grigorieva, A. A. Firsov, *Science* **2004**, *306*, 666.
[4] R. H. Baughman, H. Eckhardt, M. Kertesz, *J. Chem. Phys.* **1987**, *87*, 6687.
[5] Y. Li, L. Xu, H. Liu, Y. Li, *Chem. Soc. Rev.* **2014**, *43*, 2572.
[6] K. Srinivasu, S. K. Ghosh, *J. Phys. Chem. C* **2012**, *116*, 5951.
[7] N. Narita, S. Nagai, S. Suzuki, K. Nakao, *Phys. Rev. B* **1998**, *58*, 11009.
[8] A. N. Enyashin, A. L. Ivanovskii, *Phys. Status Solidi B* **2011**, *248*, 1879.
[9] G. Luo, X. Qian, H. Liu, R. Qin, J. Zhou, L. Li, Z. Gao, E. Wang, W. Mei, J. Lu, Y. Li, S. Nagase, *Phys. Rev. B* **2011**, *84*, 075439.
[10] M. Long, L. Tang, D. Wang, Y. Li, Z. Shuai, *ACS Nano* **2011**, *5*, 2593.
[11] Q. Zheng, G. Luo, Q. Liu, R. Quhe, J. Zheng, K. Tang, Z. Gao, S. Nagase, J. Lu, *Nanoscale* **2012**, *4*, 3990.
[12] Y. Jiao, A. Du, M. Hankel, Z. Zhu, V. Rudolph, S. C. Smith, *Chem. Commun.* **2011**, *47*, 11843.
[13] J. He, S. Ma, P. Zhou, C. Zhang, C. He, L. Sun, *J. Phys. Chem. C* **2012**, *116*, 26313.
[14] X. Gao, J. Zhou, R. Du, Z. Xie, S. Deng, R. Liu, Z. Liu, J. Zhang, *Adv. Mater.* **2016**, *28*, 168.
[15] J. Li, X. Gao, B. Liu, Q. Feng, X. Li, M. Huang, Z. Liu, J. Zhang, C. Tung, L. Wu, *J. Am. Chem. Soc.* **2016**, *138*, 3954.
[16] Y. Li, Z. Zuo, *Joule* **2019**, *3*, 899.
[17] Y. Li, Y. Xue, H. Yu, *Adv. Mater.* **2019**, *31*, 1803101.
[18] L. Hui, Y. Xue, H. Yu, Y. Liu, Y. Fang, C. Xing, B. Huang, Y. Li, *J. Am. Chem. Soc.* **2019**, *141*, 10677.
[19] Y. Xue, B. Huang, Y. Yi, Y. Guo, Z. Zuo, Y. Li, Z. Jia, H. Liu, Y. Li, *Nat. Commun.* **2018**, *9*, 1460.
[20] C. Huang, S. Zhang, H. Liu, Y. Li, G. Cui, Y. Li, *Nano Energy* **2015**, *11*, 481.
[21] G. Li, Y. Li, H. Liu, Y. Guo, Y. Li, D. Zhu, *Chem. Commun.* **2010**, *46*, 3256.
[22] J. Zhou, X. Gao, R. Liu, Z. Xie, J. Yang, S. Zhang, G. Zhang, H. Liu, Y. Li, J. Zhang, Z. Liu, *J. Am. Chem. Soc.* **2015**, *137*, 7596.
[23] Z. Zuo, H. Shang, Y. Chen, J. Li, H. Liu, Y. Li, Y. Li, *Chem. Commun.* **2017**, *53*, 8074.
[24] X. Gao, Y. Zhu, D. Yi, J. Zhou, S. Zhang, C. Yin, F. Ding, S. Zhang, X. Yi, J. Wang, L. Tong, Y. Han, Z. Liu, J. Zhang, *Sci. Adv.* **2018**, *4*, eaat6378.
[25] A. L. Ivanovskii, *Prog. Solid State Chem.* **2013**, *41*, 1.
[26] C. Huang, Y. Li, N. Wang, Y. Xue, Z. Zuo, H. Liu, Y. Li, *Chem. Rev.* **2018**, *118*, 7744.
[27] R. R. Mishra, A. K. Sharma, *Composites, Part A* **2016**, *81*, 78.
[28] X. Qian, H. Liu, C. Huang, S. Chen, L. Zhang, Y. Li, J. Wang, Y. Li, *Sci. Rep.* **2015**, *5*, 7756.
[29] C. Li, X. Lu, Y. Han, S. Tang, Y. Ding, R. Liu, H. Bao, Y. Li, J. Luo, T. Lu, *Nano Res.* **2018**, *11*, 1714.
[30] S. Zhang, J. Wang, Z. Li, R. Zhao, L. Tong, Z. Liu, J. Zhang, Z. Liu, *J. Phys. Chem. C* **2016**, *120*, 10605.
[31] A. C. Ferrari, J. C. Meyer, V. Scardaci, C. Casiraghi, M. Lazzeri, F. Mauri, S. Piscanec, D. Jiang, K. S. Novoselov, S. Roth, A. K. Geim, *Phys. Rev. Lett.* **2006**, *97*, 187401.
[32] J. Zhong, J. Wang, J. Zhou, B. Mao, C. Liu, H. Liu, Y. Li, T. Sham, X. Sun, S. Wang, *J. Phys. Chem. C* **2013**, *117*, 5931.
[33] T. Mabuchi, H. Toda, H. Yamanaka, *J. Phys. Soc. Jpn.* **1993**, *62*, 246.
[34] M. Larhed, C. Moberg, A. Hallberg, *Acc. Chem. Res.* **2002**, *35*, 717.
[35] M. Drev, U. Grošelj, B. Ledinek, F. Perdih, J. Svete, B. Stefane, F. Požgan, *ChemCatChem* **2018**, *10*, 3824.
[36] Y. Cai, A. Jalan, A. R. Kubosumi, S. L. Castle, *Org. Lett.* **2015**, *17*, 488.
[37] B. Radisavljevic, A. Radenovic, J. Brivio, V. Giacometti, A. Kis, *Nat. Nanotechnol.* **2011**, *6*, 147.

© 2020 WILEY-VCH Verlag GmbH & Co. KGaA, Weinheim

16163028, 2020, 23, Downloaded from https://onlinelibrary.wiley.com/doi/10.1002/adfm.202001396 by Zhejiang University, Wiley Online Library on [04/09/2023]. See the Terms and Conditions (https://onlinelibrary.wiley.com/terms-and-conditions) on Wiley Online Library for rules of use; OA articles are governed by the applicable Creative Commons License